Max-Planck-Institut
für Meteorologie

REPORT No. 21

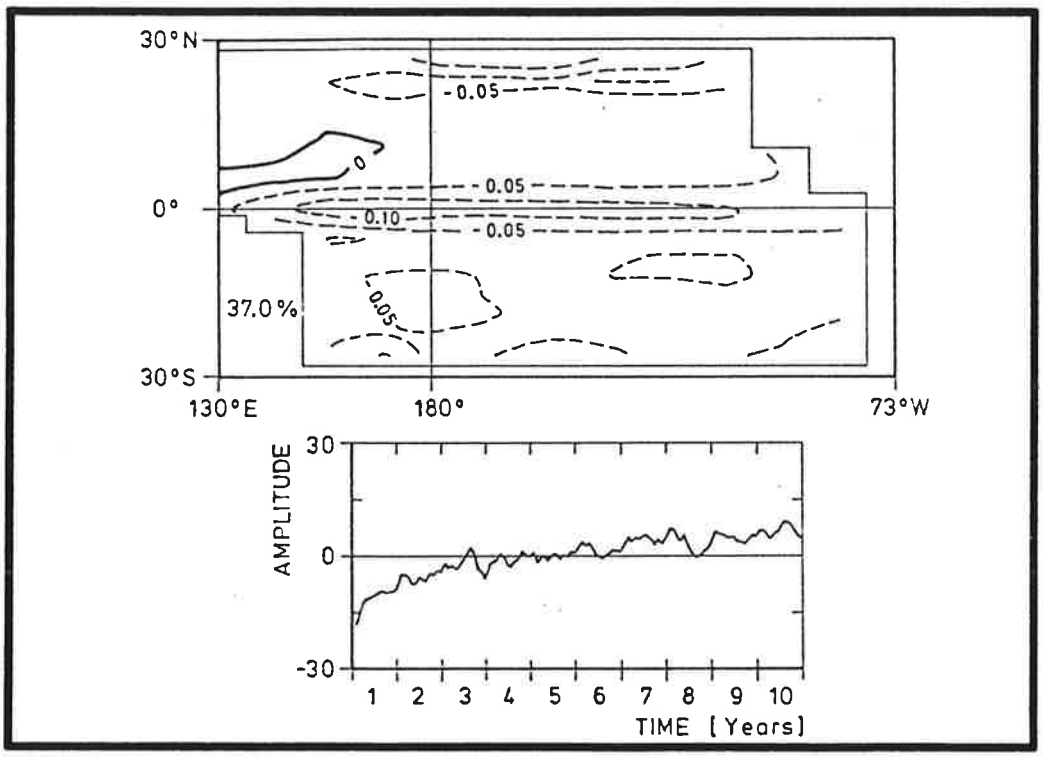

A TEN YEAR CLIMATE SIMULATION WITH A COUPLED OCEAN–ATMOSPHERE GENERAL CIRCULATION MODEL

by

M. LATIF • J. BIERCAMP • H. VON STORCH • F.W. ZWIERS

HAMBURG, OCTOBER 1988

AUTHORS:

MOJIB LATIF
MAX-PLANCK-INSTITUT
FUER METEOROLOGIE

JOACHIM BIERCAMP
MAX-PLANCK-INSTITUT
FUER METEOROLOGIE

HANS VON STORCH
MAX-PLANCK-INSTITUT
FUER METEOROLOGIE

FRANCIS W. ZWIERS
CANADIAN CLIMATE CENTRE
4905 DUFFERIN STREET, DOWNSVIEW
ONTARIO
M3H 5T4, CANADA

MAX-PLANCK-INSTITUT
FUER METEOROLOGIE
BUNDESSTRASSE 55
D-2000 HAMBURG 13
F.R. GERMANY

Tel.: (040) 4 11 73-0
Telex: 211092
Telemail: MPI.Meteorology
Telefax: (040) 4 11 73-298

A TEN YEAR CLIMATE SIMULATION
WITH A
COUPLED OCEAN-ATMOSPHERE GENERAL CIRCULATION MODEL

M. Latif, J. Biercamp, H. von Storch,and F. W. Zwiers*

Max-Planck-Institut für Meteorologie
Bundesstraße 55, D 2000 Hamburg 13, F.R.G.

*Canadian Climate Centre
4905 Dufferin Street, Downsview, Ontario, M3H 5T4, Canada

ABSTRACT

A coupled ocean-atmosphere general circulation model consisting of a regional model of the Tropical Pacific Ocean and a global low resolution atmospheric model was integrated for ten years. The results show that there is a significant trend in the climate of the coupled model which may be characterized by a gradual cooling of the upper ocean in the near equatorial region. This oceanic cooling is associated with changes of the atmospheric circulation reminiscent of anomalies connected with the occurence of cold equatorial Pacific SST anomalies.

The annual mean atmospheric and oceanic circulation are reasonably well simulated as are the phase and the patterns of the annual cycle. However, the amplitudes of the annual cycle are significantly underestimated. The cooling of the Equatorial Pacific apparently reduces atmospheric variability on all time scales. In particular, the model does not oscillate on the El Niño/ Southern Oscillation time scale of a few years.

1. INTRODUCTION

Low-frequency variability in the tropics strongly depends on large scale interactions between ocean and atmosphere in this region. These air-sea interactions, which are found on annual as well as on interannual time scales, are most obvious during El Niño/Southern Oscillation (ENSO) events, when anomalously warm waters appear in the upper Equatorial Pacific (Gill and Rasmusson, 1983) for several months. Because of these crucial large scale air-sea interactions any simulation of tropical low-frequency variability must be done with a model which describes both the ocean and the atmosphere and their interactions explicitly. Presently, such coupled ocean-atmosphere models are developed at different institutions (e. g. Philander, pers. commu., Gordon, pers. commu.). The purpose of this paper is to briefly describe such a coupled ocean-atmosphere model and its performance in a ten year extended integration.

The paper focuses on the following questions:

1) Does the simulated climate contain significant trends, and if so, how do they affect the atmospheric and oceanic circulation?

2) How well does the coupled model simulate the annual mean circulation and the annual cycle?

3) Does the coupled model show low frequency variations of the El Niño/ Southern Oscillation (ENSO) type?

The oceanic and atmospheric components of the coupled model and the coupling technique are described in Section 2 of the paper. Results of the ten year extended integration conducted with the model are presented in Section 3. The paper is concluded in Section 4 with a summary and discussion of the results.

2. THE COUPLED OCEAN-ATMOSPHERE MODEL

The coupled model consists of a regional model of the Tropical Pacific Ocean and a global atmospheric model. A slightly different version of this model was used to investigate the response of the coupled system to wind bursts over the Western Equatorial Pacific (Latif et al., 1988).

The ocean model, described in detail in Latif (1987), is a primitive equation model which resolves the Tropical Pacific Ocean from 30°N to 30°S and from 130°E to 70°W. The model includes real coastlines but does not incorporate bottom topography; the ocean floor is at a constant depth of 4000 m. The zonal resolution is constant at 670 km, while the meridional resolution is variable, increasing from 50 km near the equator to approximately 400 km at the boundaries. There are 13 levels in the vertical, ten of which are placed within the upper 300 m of the ocean. In contrast to Latif (1987), we adopt Richardson number dependent mixing coefficients (Pacanowsky and Philander, 1981). The vertical eddy viscosity and eddy diffusivity were both assigned values of 20 cm^2/s under neutral conditions and have background values of 0.1 and 0.01 cm^2/s respectively. The horizontal eddy viscosity is constant with a value of 10^8 cm^2/s. Explicit horizontal heat diffusion is not included.

The design of the atmospheric model and its ability to reproduce the observed atmospheric circulation are described in a series of contributions contained in two reports (Fischer, 1987; Storch, 1988). This spectral model is integrated in the spectral domain spanned by the T21-resolution, i.e., a maximum of 21 zonal wavenumbers is resolved. The nonlinear terms and the parameterized physcial processes are calculated on the 64 x 32 Gausian grid which yields a horizontal resolution of about 5.6°. There are 16 levels in the vertical which are defined on σ-surfaces in the lower troposphere and on p-surfaces in the upper troposphere and in the stratosphere.

The coupling technique which allows the two models to interact is sketched in Fig. 1. The ocean model is driven by turbulent surface momentum and heat fluxes which are computed by the atmospheric model. The atmospheric model in turn is influenced by SST, which is simulated over the Tropical Pacific by the ocean model and specified from climatology elsewhere. As in the flux correction scheme suggested by Sausen et al. (1988), we correct all three interactive quantities with seasonally varying offset values determined from

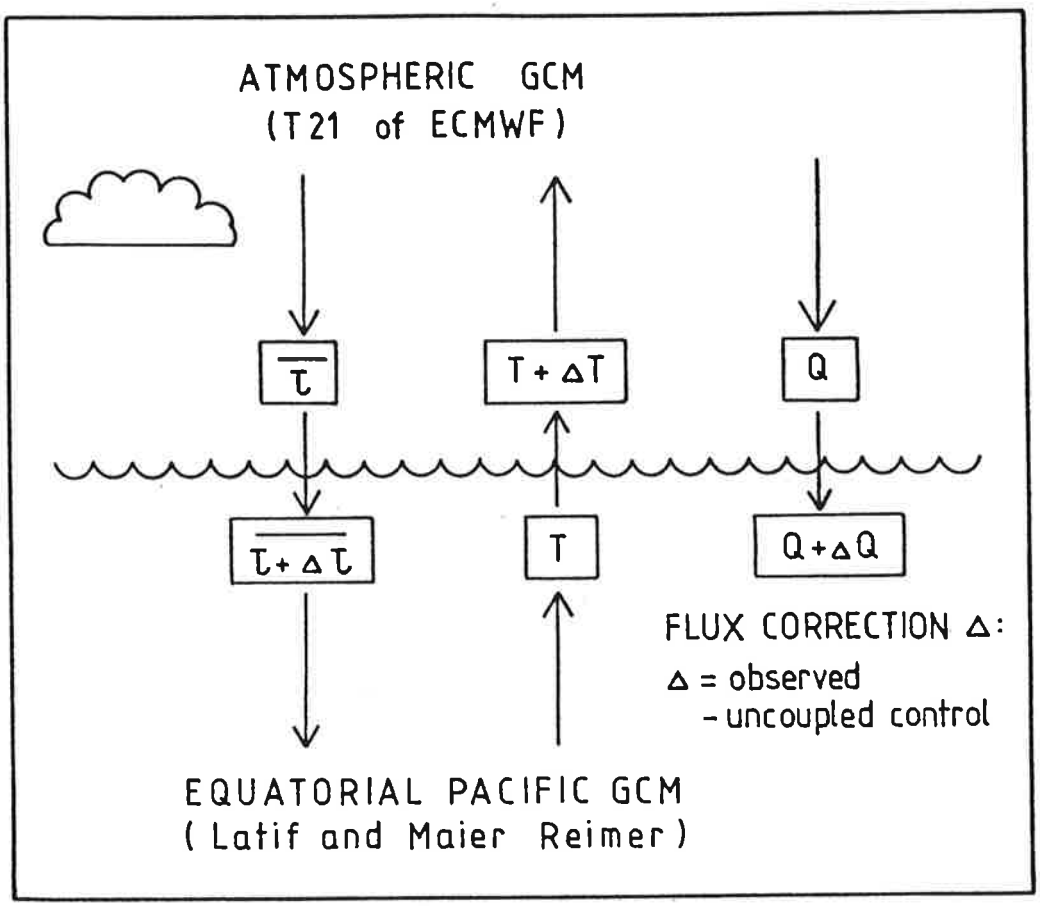

Figure 1:

Sketch of the technique to couple the atmospheric and the oceanic GCMs. The net heat flux Q and the wind stress τ are calculated by the atmospheric model, and the SST T by the oceanic model. The correction terms ΔQ, $\Delta\tau$ and ΔT are derived from observations and uncoupled runs of the oceanic and atmospheric models. In the coupled model, the oceanic component is forced with the "corrected" heat and momentum fluxes, $Q+\Delta Q$ and $\tau+\Delta\tau$, and the atmospheric component with the "corrected" SST, $T+\Delta T$.

uncoupled control runs which used climatological forcing. The correction terms are equal to the model errors (observation - simulation) and are shown for January in Fig. 2. The spatial error patterns are generally the same for all months.

The SST correction pattern ΔT, shown in Fig. 2a, has a belt of positive values in the equatorial region with a maximum of approximately $1^{\circ}C$, indicating that the uncoupled model simulates lower than observed SSTs in this region. In other months (not shown) this effect is even stronger with errors of up to $2^{\circ}C$. In all other regions the uncoupled ocean model simulates higher than observed temperatures with maximum errors of about $2^{\circ}C$.

Surface wind stress corrections $\Delta\tau$, shown in Figs. 2b and c, were calculated using Goldenberg's and O'Brien's (1981) dataset with a drag coefficient of 1.5×10^{-3} and air density of 1.2 kg/m^3. The patterns show clearly that this quantity is underestimated by the uncoupled atmospheric model. As was shown by Biercamp and Storch (1987) in an analysis of a ten year uncoupled control run, the spatial structure of the surface wind stress patterns are reasonably well simulated by the atmospheric model. However, their amplitudes are much too weak. The resulting stress corrections are therefore of the same order of magnitude as the simulation itself (even stronger in the case of the meridional wind stress component).

The estimation of the flux correction ΔQ for the surface heat flux is computed slightly differently because the ocean model is not forced by observed heat fluxes during the uncoupled control run. Instead, we applied a Newtonian cooling type flux parameterization using a temperature $2^{\circ}C$ larger than the climatological air temperature at 2 m height and a time constant of about 30 days for the upper layer's thickness of 10 m. The heat flux going into the ocean which is derived by applying this formula is referred to as "observed" heat flux. We subtract the net surface heat flux from the atmospheric model from this "observed" flux . The resulting flux correction term for January is shown in Fig. 2d. The largest corrections are made in the Eastern and Southeastern Pacific, where the atmospheric model gives much larger heat fluxes than those determined from the oceanic model.

The integration begins on a January 1, using atmospheric and oceanic initial fields simulated in the uncoupled model's runs.

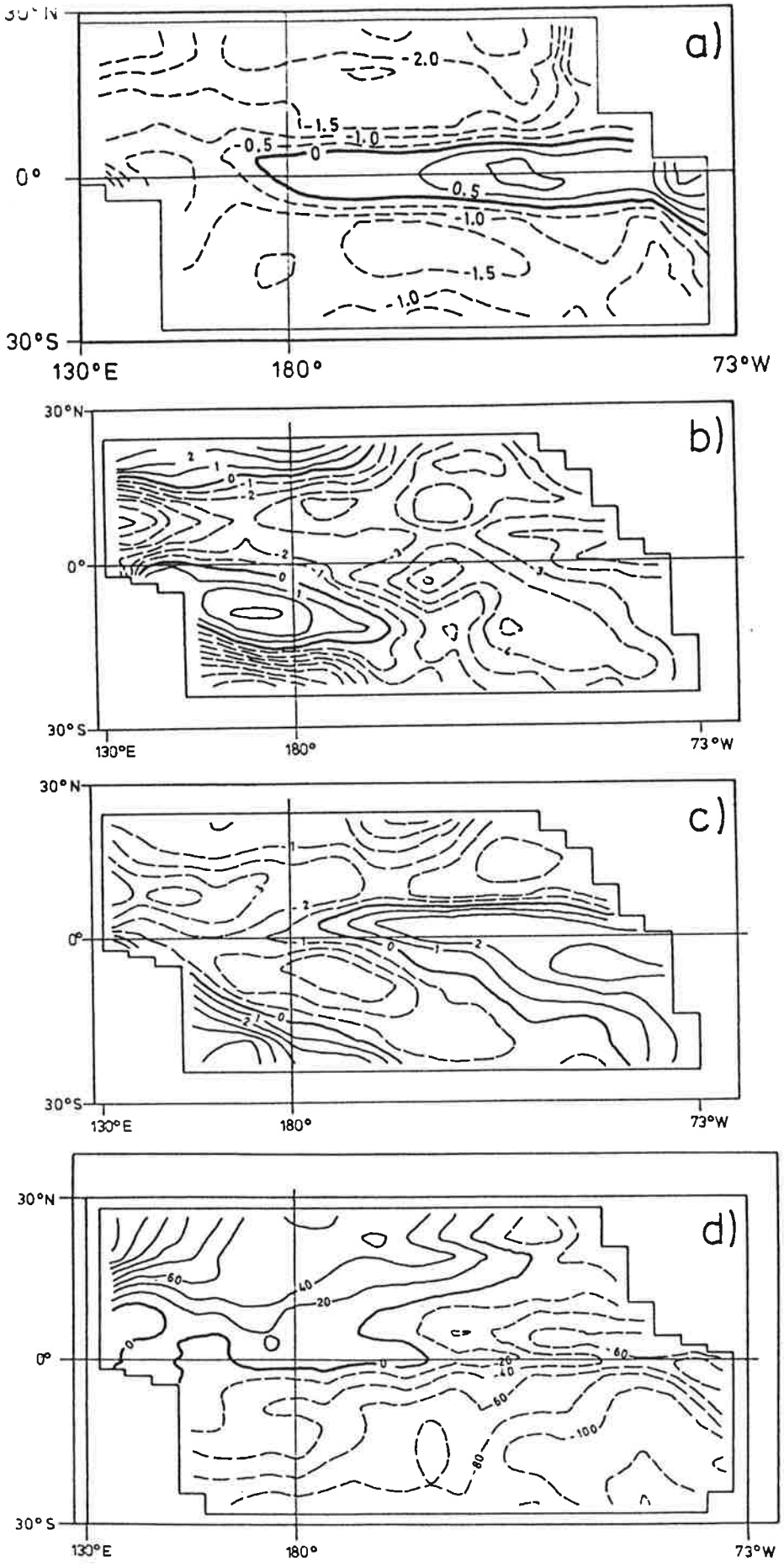

Figure 2:

Flux corrections for January

a) for SST, ΔT ($^{\circ}C$)

b) for zonal wind stress, $\Delta\tau_x$ (0.1 mPa)

c) for meridional wind stress, $\Delta\tau_y$ (0.1 mPa)

d) for net surface heat flux, ΔQ (Wm^{-2}).

3. RESULTS

3.1 Climate Trend

The most obvious result of the ten year integration is its climate trend. The entire equatorial ocean experiences a continous cooling which is connected with atmospheric anomalies somewhat analogous to a cold event of the SO. The trend in simulated SST can easily be seen by considering EOF coefficient time series. The leading EOF of simulated SST after removal of the annual cycle is displayed in Fig. 3a. This mode accounts for 37% of the total variance of SST not attributable to the annual cycle. The corresponding coefficient time series, which is shown in Fig.3b, clearly exhibits an increasing trend in SST. In the Equatorial Pacific, where the EOF is large and negative, there is a substantial downward trend in SST which dominates the variability of SST in this region. The spatial pattern of the cooling is almost zonally symmetric. Maximum cooling occurs directly on the equator with values of more than $3^{\circ}C$ in 10 years. The ocean cools more quickly during the first two years of the integration than during the subsequent 8 years. During the last 8 years the trend has almost constant slope. In contrast to the equatorial region there is a tendency for a slight increase in SST at higher latitudes.

When analyzing the inter-annual variance of SST simulated by the coupled model one has to take the rather strong trend into account. This was done by fitting second degree polynomials to the simulated mean seasonal SSTs averaged over the grid boxes of the atmospheric model. The use of an exponentially decaying trend model may have been preferable but was avoided due to the complexity of solving non-linear least squares problems at hundreds of grid points. The methodology used to fit the polynomials and assess their statistical significance is described in Zwiers (1988).

Our calculations (not shown) indicate that the trend in SST is highly significant within 5° latitude of the equator over much of the Pacific. Simulated JJA (June, July, August) mean SST anomalies in two sample atmospheric grid boxes are displayed in Fig. 4 together with the fitted trend. These diagrams, which are typical of seasonal mean SST anomalies simulated near the equator (Fig. 4a) and away from the equator (Fig. 4b), demonstrate the relative contributions of trend and low-frequency variability to simulated SST inter-annual variability at equatorial and non-equatorial locations.

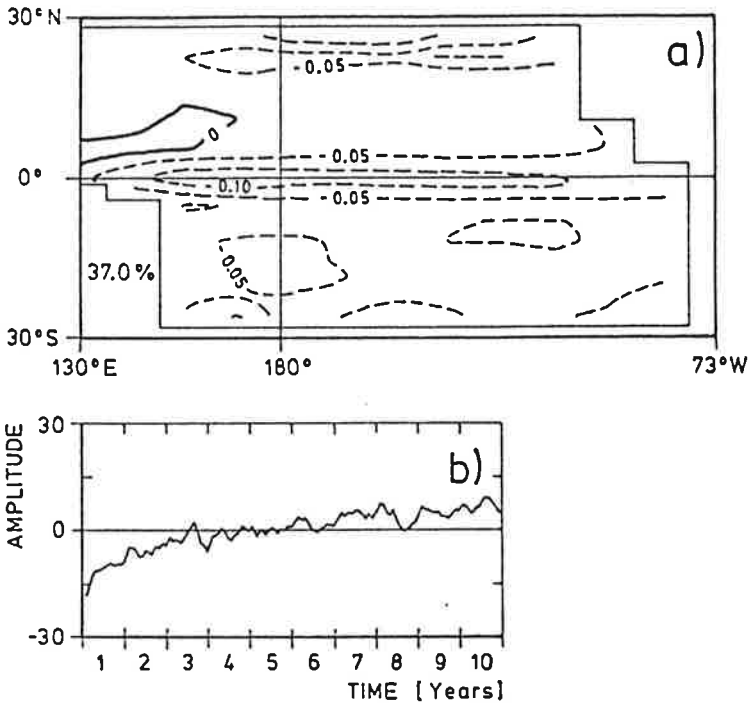

Figure 3:
First EOF of simulated SST after removal of the annual cycle (a) and its coefficient time series (b). This mode accounts for 37% of the total variance. Units of pattern: °C.

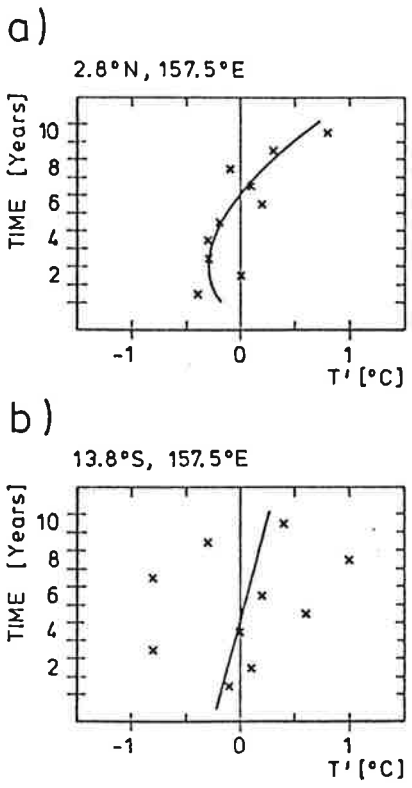

Figure 4:
Simulated JJA SST anomalies in two grid boxes centered at approximately 157.5°E, 2.8°N (a) and at 157.5°E, 13.8°S. The solid curve shows the fitted trend.

The temporal evolution in the equatorial box centered at 157.5°E and 2.8°N (Fig. 4a) is typical of all seasons and most locations near the equator in the Pacific. The data reveal a relatively large decrease in SST between years one and two and then an almost linear decrease of about 0.6°C during the subsequent 9 years. The fitted polynomial does an adequate job of representing this behaviour. Apparently little inter-annual variability is left in the simulated seasonal mean SSTs after the removal of the trend. In fact, estimates of inter-annual variance taking trend into account(not shown) near the equator are approximately one order of magnitude lower than estimates of observed inter-annual variance reported by Shea (1986).

The partitioning of inter-annual variance into trend and low-frequency variance components at grid boxes near the equator which was illustrated above differs markedly from that at locations off the equator. Outside the equatorial band the trend is much weaker and inter-annual variance about the trend is of the same order of magnitude as in the observations (Shea, 1986). This is illustrated in Fig. 4b with the JJA SST anomalies in the atmospheric grid box centered at 157.5°E and 13.8°S. There is a small linear decreasing trend of about 0.5°C over 10 years and the SSTs vary irregularly about the trend with an estimated standard deviation of about 0.5°C.

A similar decrease in SST within the narrow equatorial belt was seen in a ten year integration of the ocean model run in an uncoupled mode. In contrast to the coupled integration, the uncoupled ocean model was forced with climatological wind stress and a heat flux determined from the last seasonal cycle of the spin up integration. Therefore, the trend observed in SST simulated in the coupled run may be attributed primarily to the ocean model, which due to its closed basin, does not contain the processes which are necessary to maintain the thermocline. Consequently the initial stratification of the ocean is gradually destroyed by explicit and numerical heat diffusion, leading to a cooling of the upper layers and a warming in the deep ocean.

The atmospheric model responds to the cooling of the upper ocean layers with an increase of net surface heat flux. This can be inferred from Fig. 5 which displays the first EOF of net surface heat flux and its coefficient time series. This EOF accounts for about 10% of the total variance. Its spatial pattern (Fig. 5a) has large values in the equatorial region with peak values in the western part. Note that the EOF is negative in the equatorial region

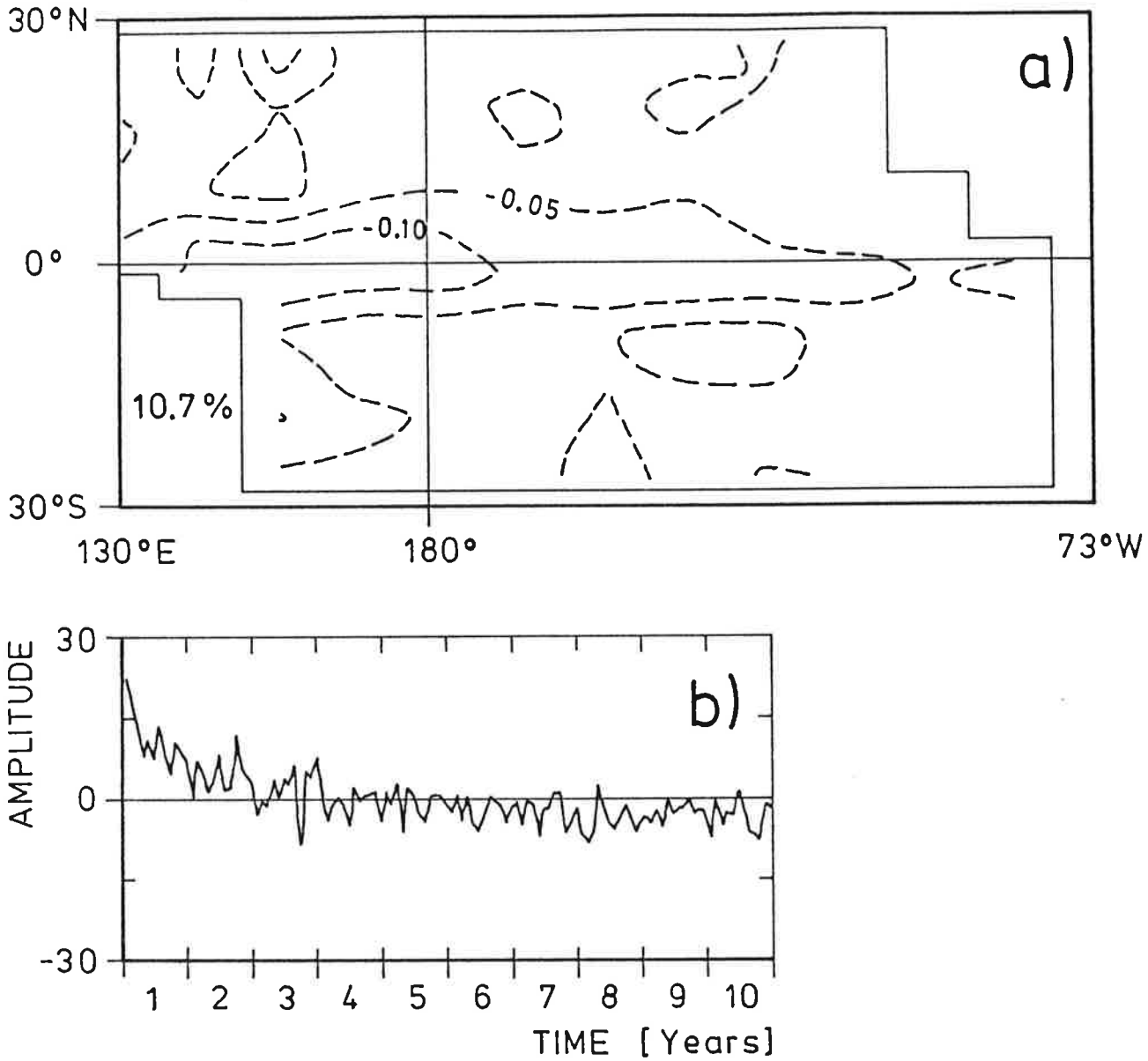

Figure 5:

First EOF of simulated net heat flux, Q, after removal of the annual cycle (a) and its coefficient time series (b). This mode accounts for 10% of the total variance. Units of pattern: Wm^{-2}.

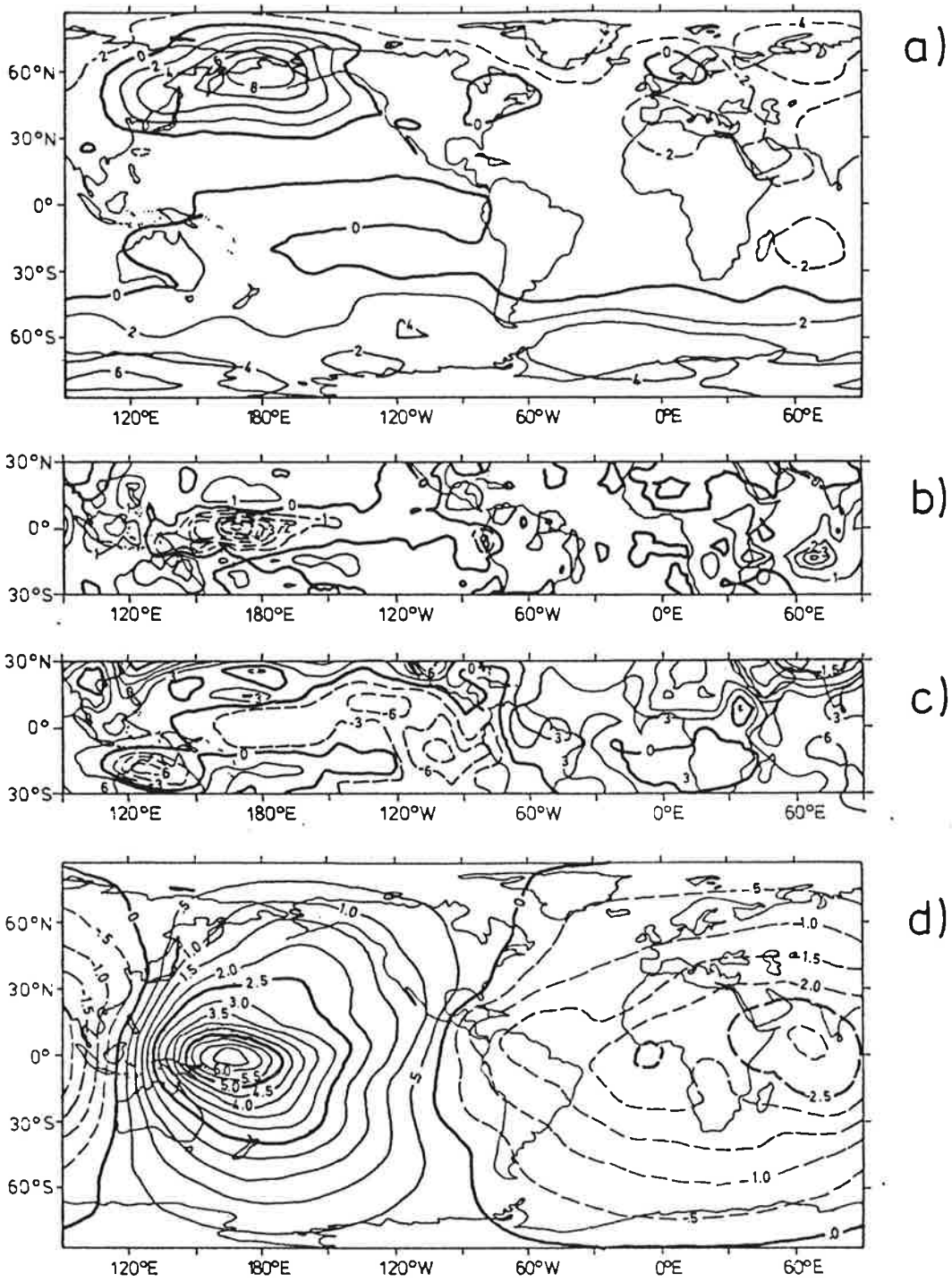

Figure 6:

10 year mean DJF differences between some atmospheric quantities simulated with the coupled and with the uncoupled atmospheric model.

a) sea level pressure (hPa),

b) precipitation (mm/day),

c) 850 hPa temperature (^{o}C),

d) velocity potential at 300 hPa (10^{6} $m^{2}s^{-1}$).

The zero contour is emboldened, negative deviations given by dashed lines and positive deviations by solid lines.

and that the coefficients decrease in time resulting in negative coefficients after about 24 months. Thus, the EOF describes an increase of the net surface heat flux which ranges from about 20 W/m^2 in the Eastern Equatorial Pacific to approximately 80 W/m^2 in the western part. Most of the changes in net surface heat flux occur during the first year as is shown in Fig. 5b. Due to feedback from the atmospheric model the rate of cooling of the ocean decreases with time (see Figs. 4b and 14a) with the result that the decrease of SST in the coupled run is less than that in the run with the uncoupled ocean model mentioned in the preceding paragraph.

The cooling of the Equatorial Pacific Ocean's surface is reflected in atmospheric quantities such as sea level pressure (SLP), rainfall, 850 hPa temperature and 300 hPa velocity potential. The mean DJF (December, January, February) differences in these quantities between the coupled and uncoupled runs are shown in Fig. 6.

Locally, i.e., in the vicinity of the cooled ocean's surface, the atmosphere reacts with strongly decreased rainfall (Fig. 6b) and decreased 850 hPa temperature (Fig. 6c). Maximum precipitation deficits occur slightly to the west of the dateline with values of about 7 mm/day. The lower troposphere is considerably cooler over the Tropical Pacific. Maximum temperature differences of about 0.3°C are found at the dateline .

The upward branch of the Walker Cell is strongly weakened, as can be inferred from the reduced difluence at the 300 hPa level (Fig. 6d). Interestingly, similar features are also present in a simulation of the impact of cold equatorial SST anomalies (Cubasch, 1985). Therefore, the differences between the coupled and the uncoupled atmospheric simulation may be understood in part as an atmospheric reaction to anomalous SST.

It is not surprising that there are also remote changes in the atmospheric state which correspond to the strong changes in local circulation described above. In particular SLP is reduced by as much as -2 hPa in the tropics outside the Pacific Ocean where no surface cooling takes place (Fig. 6a) and excess rainfall of up to 4 mm/day is found over the Indian Ocean (Fig. 6b). The reduced upper air difluence of the upward branch of the Walker cell is balanced by enhanced difluence over the western Indian Ocean and the Eastern Alantic Ocean (Fig. 6d). There are increased 850 hPa temperatures with maximum

deviations of 0.3° to 0.6°C over the Indian ocean (Fig. 6c). SLP also shows a remote response in the North Pacific sector. This SLP response pattern, which is reminiscent of the negative PNA, appears most strongly in winter and is absent in summer. This is in full accord with a finding of Barnston and Livezey (1987), who identified the PNA as an anomaly pattern which is excited in all seasons except Northern summer. These remote differences are also reminiscent of anomalies found by Cubasch (1985) when forcing the uncoupled atmospheric model with a negative SST anomaly in the Equatorial Pacific.

The atmospheric response to the cooling ocean appears as a trend in many variables because the cooling of the ocean is a continous process . The pattern of the trend in 300 hPa velocity potential is very large-scaled. Large positive linear trends of up to $3 \cdot 10^6$ $m^2 s^{-1} year^{-1}$ are observed over the Western Tropical Pacific during both extreme seasons and corresponding large negative trends can be seen in the opposite hemisphere.

The change in the general atmospheric circulation is summarized in Fig. 7 which shows the zonally averaged vertical velocity as it evolves during the integration. A region of downward motion develops on the equator in response to the cooling of the underlying ocean. This leads to a division of the upward branch of the Hadley Circulation into two parts. This downward motion has considerable vertical extent and is consistent with a reduction of the strength of the Hadley Circulation in the beginning of the integration, and partly with its reversal as the integration is continued.

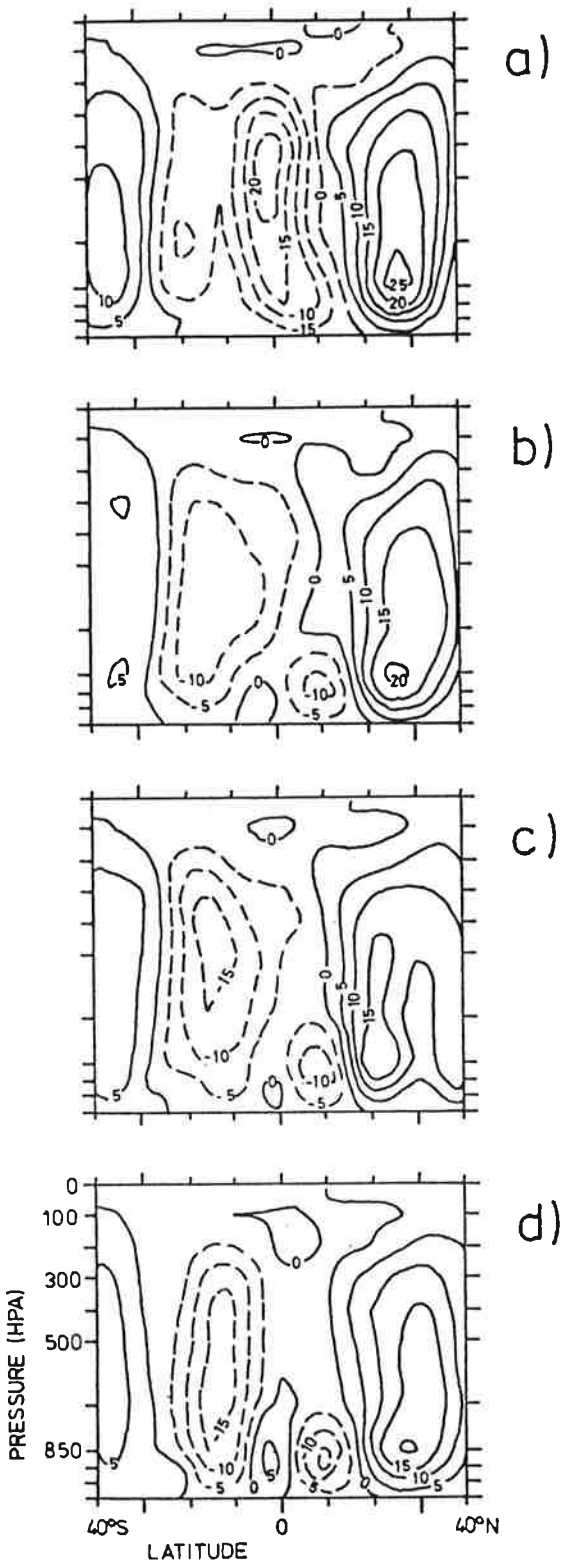

Figure 7:

Monthly mean zonally averaged vertical velocity for January of a) year 1, b) year 2, c) year 5, and d) year 10 of the coupled integrations. Units: hPa/s. Upward motion is given by dashed lines and downward motion by solid lines.

3.2 Annual Mean Fields

Due to the climate trend described above, the simulated annual mean SST shows significant deviations from the observed pattern which are most obvious in the equatorial region. The simulated SSTs (not shown) exhibit a very strong equatorial cold tongue. Maximum errors occur in the Central Pacific with values of about 4°C. In all other regions the model simulated SSTs show reasonable agreement with the observations.

Sea level is simulated with more success than SST as can been seen from Figs. 8a and b which display observed and simulated sea level . The simulated sea level slope along the equator of about 50 cm compares favourably with observations. Also, the counter current trough and subtropical highs are simulated at about the observed locations and with the observed strength. The fact that sea level slope is correctly simulated along the equator further supports the view that the gradual cooling of equatorial SST is not caused by an intensification of the Trade Winds and subsequently enhanced equatorial upwelling.

The simulated annual mean wind stress shows essentially the same features as described by Biercamp and Storch (1987) for the uncoupled ten year control run. The coupled run simulates the patterns realistically but underestimates the ampitudes markedly. For instance, the two maximum regions associated with the centers of the Northeast and Southeast Trades are well represented in the coupled model simulation, but the strengths are only about 50% of the observed strengths.

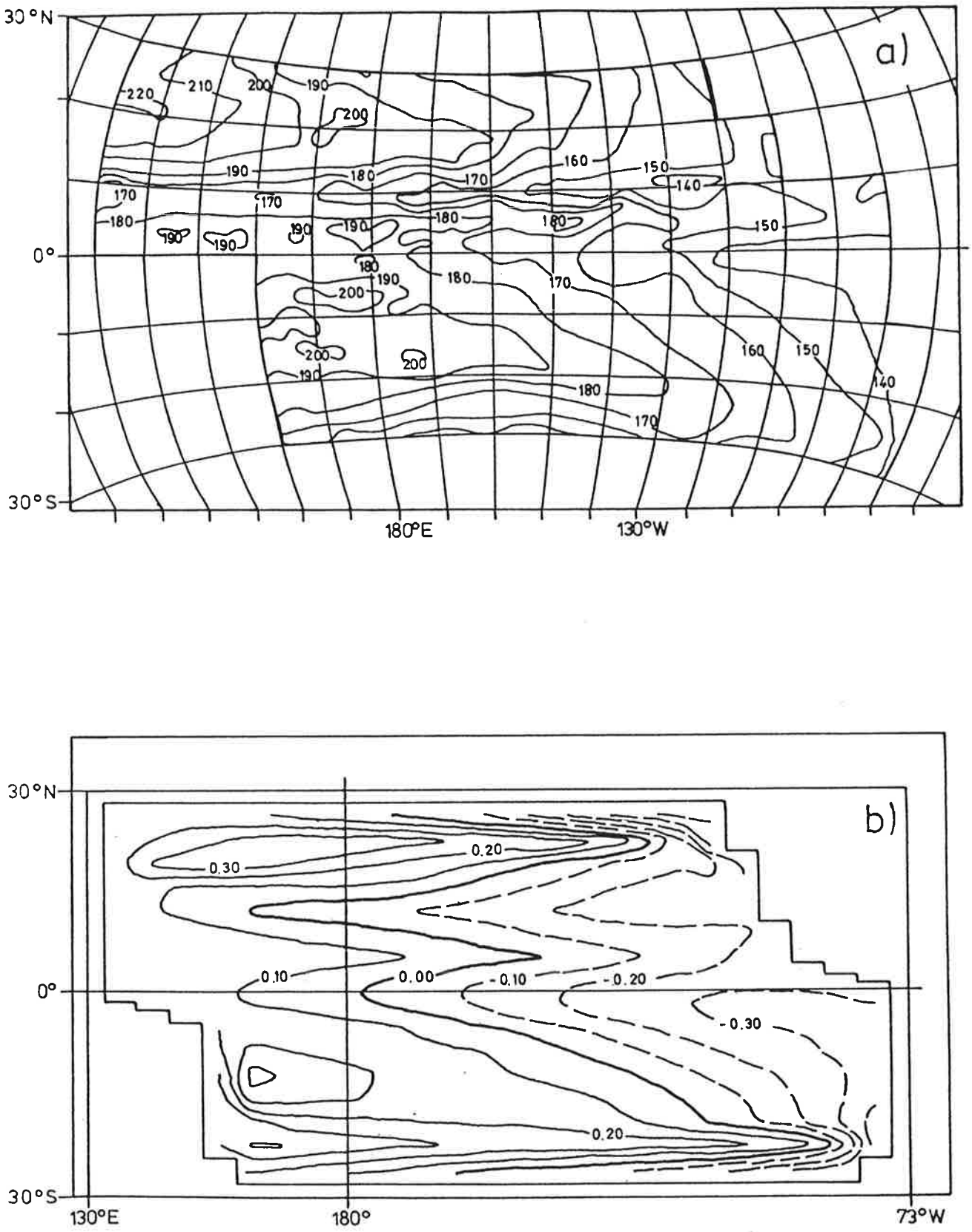

Figure 8:

Annual mean observed (a) and simulated (b) sea level in the tropical Pacific. The observations are taken from Wyrtki (1974). Contour Interval: 0.1 m for simulation, 10 cm for observation.

3.3 Annual Cycle

We restrict our description of the annual cycle to zonal wind stress and SST because these two variables are the most important quantities in air-sea interaction. We consider EOFs derived from data which include the annual cycle. Therefore, the first EOF will, in most cases, describe the annual cycle, because it generally contributes most heavily to the total variance.

Figs. 9a and 10a show the first EOFs of observed (Goldenberg and O'Brien, 1981) and simulated zonal wind stress. Both modes may be identified with the annual cycle as can be inferred from the coefficient time series shown in Figs. 9b and 10b. The explained variance amounts to about 32% in the observed and to 34% in the model data. The observed pattern has three regions of strong annual change which are centered in the Western Pacific at 15°N and at 15°S, and in the Central Pacific at 15°N. In the simulated patterns there are also two Western Pacific maxima, which correspond roughly to the two western regions identified in the observations. However, the third observed maximum in the Central Pacific is not well represented, possibly because of limited horizontal resolution. While the patterns (Figs. 9a, 10a) have similar amplitudes in the centers of action, the coefficient time series shown in Figs. 9b and 10b indicate that the modelled amplitude of seasonal variations is about 20% less than the observed amplitude.

The leading EOFs and their coefficient time series as obtained from observed and simulated SST are shown in Figs. 11 and 12. The observed and the simulated patterns in Figs. 11a and 12a are very similar; both have maxima in the Northwestern and Southwestern Tropical Pacific which are separated by a minimum region in the Western and Central Equatorial Pacific. As with the zonal wind stress, the amplitude of the simulated annual SST variation is significantly smaller than the observed variation. This under-estimation is most obvious in the Southeastern Pacific, where the maximum seasonal changes are of the order of 4°C in the observed data, but are not greater than 3°C in the model simulation.

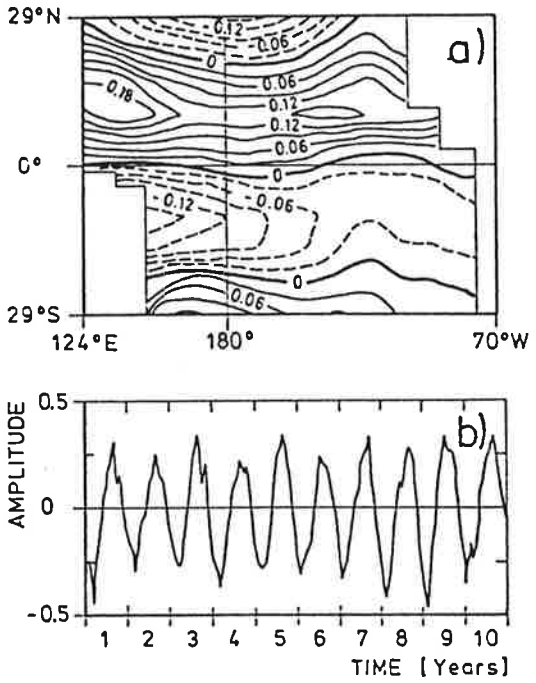

Figure 9:

First EOF of observed zonal wind stress τ_x and its coefficient time series. The data have been derived from the Goldenberg and O'Brien dataset (1981). This mode accounts for 32% of the total variance.

a) pattern (mPa)

b) time series of the pattern shown in (a).

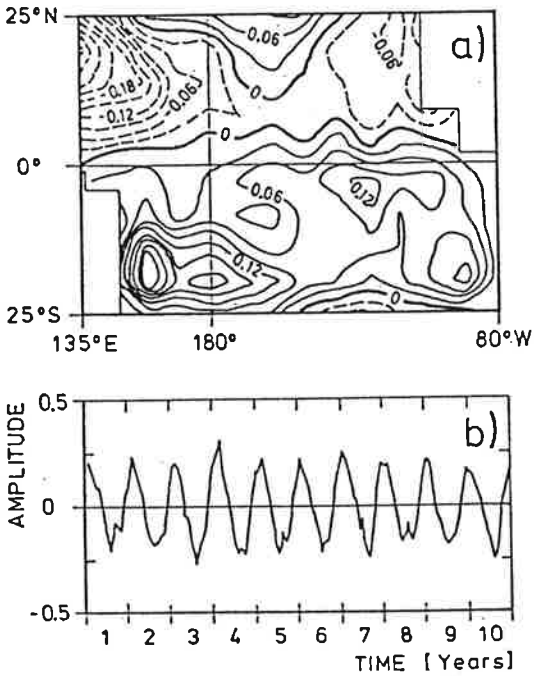

Figure 10:

First EOF of simulated zonal wind stress τ_x and its coefficient time series. This mode accounts for 34% of the total variance.

a) pattern (mPa)

b) time series of pattern shown in (a) for the 10 years of integrations.

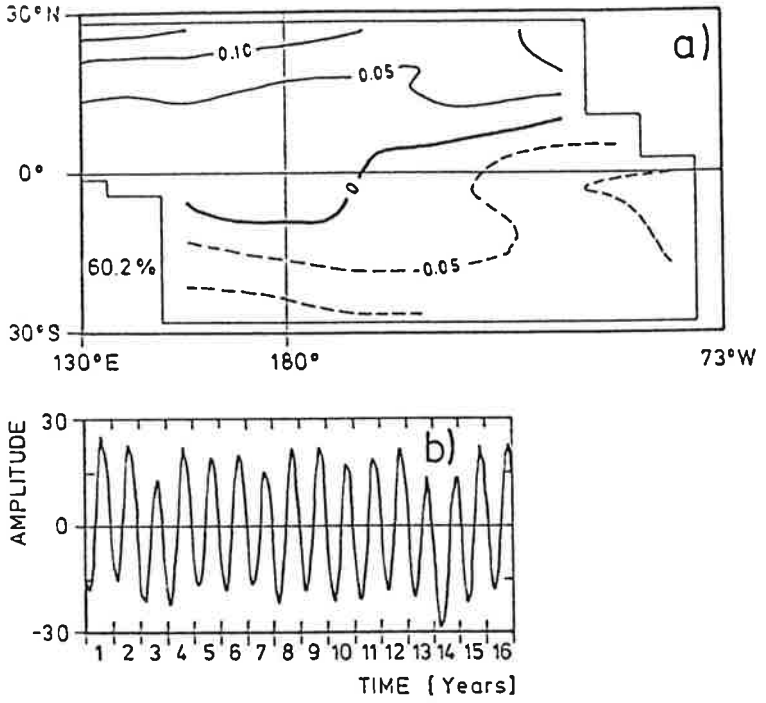

Figure 11:

First EOF of observed SST and its coefficient time series. This mode accounts for 60.2 % of the total variance

a) pattern (°C)

b) time series of the pattern shown in (a) from 1950 to 1973.

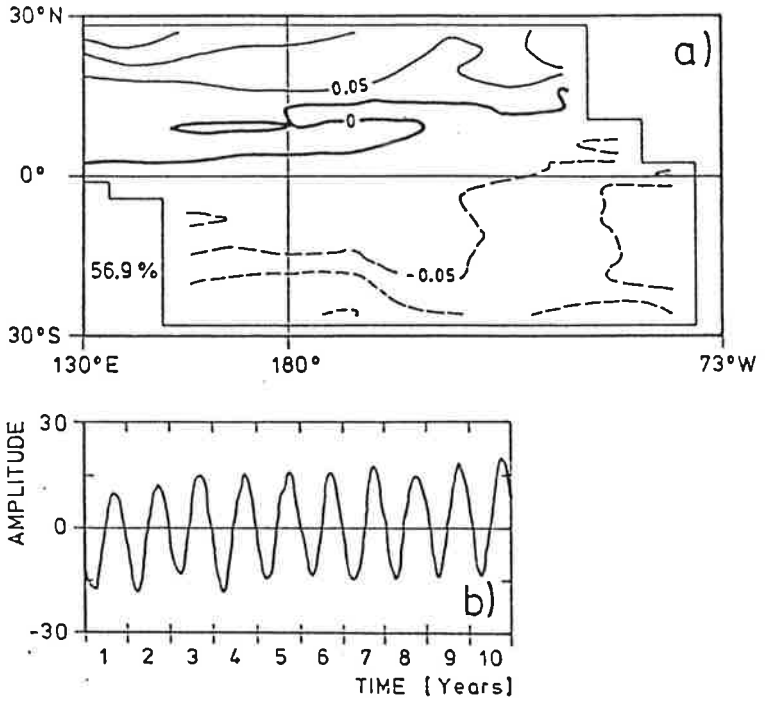

Figure 12:

First EOF of simulated SST and its coefficient time series. This mode accounts for 56.9 % of the total variance.

a) pattern (°C)

b) time series of pattern shown in (a) for the 10 years of integrations.

3.4 Interannual Variability

The characteristics of the variability of the simulated Equatorial Pacific SST can be inferred from the Hovmøller diagrams displayed in Fig. 13. Apparently changes in SST are dominated by the cooling trend and by the annual cycle. As can be seen from Fig. 13a, the interannual variability is weak. In particular, no eastward excursions or westward retreats of the warm surface waters occur in the Central Pacific as is typical for this region. The standard deviation of monthly mean SST anomalies on the equator is only of the order of a few tenths of a degree (see also Figs. 3 and 4). A Hovmøller diagram of low pass filtered SST is displayed in Fig. 13b to show the interannual variability in some more detail. In general, the low-frequency anomalies do not exceed 0.5°C and are often confined to a small longitude band. A destinct propagation of anomalies is not found. The relatively large anomaly at the beginning of the integration can be attributed to the rapid initial cooling of the simulated ocean. Except for this anomaly, the strongest event occurred during year five, when a positive SST anomaly of 0.6°C develops in the western Pacific. However, this anomaly is strongly damped with increasing longitude.

The equatorial sea level and its zonal gradient are nearly free of a trend and have negligible annual variation. The interannual variability of sea level is also small (Fig. 14). This behavior is consistent with a wind stress field which has weak variability. The equatorial zonal wind stress does not show the intense westerly wind bursts over the Western Pacific which could initiate oceanic variations. The absence of any noteworthy anomalous forcing is also reflected in the time evolution of zonal currents (not shown) which shows neither eastward surface jets nor break downs of the Equatorial Undercurrent as reported by Firring et al. (1983) for the 1982/1983 ENSO event.

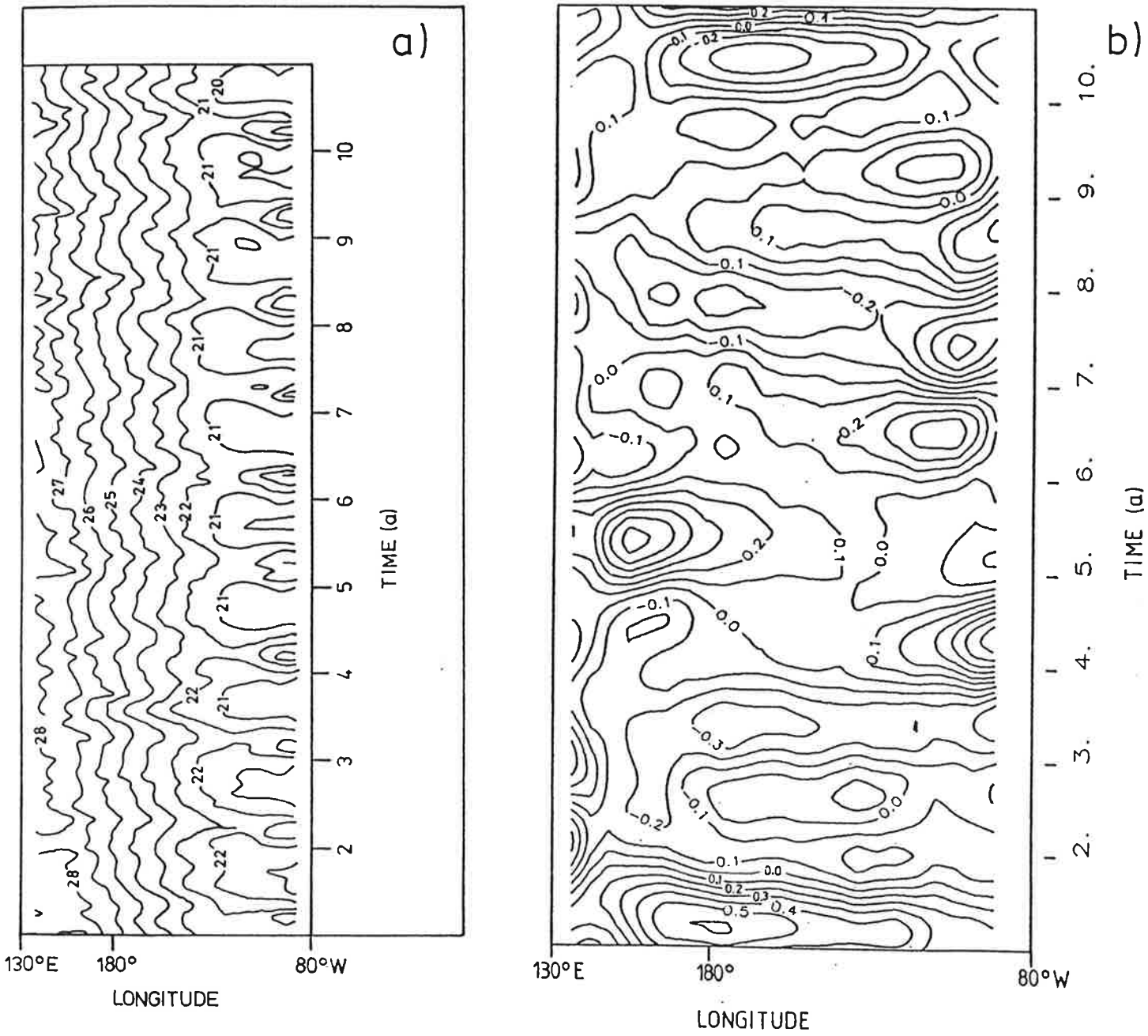

Figure 13:

Hovmøller diagrams along the equator for simulated SST.

(a) unfiltered SST; contour interval 1°C,

(b) low-pass filtered SST - the linear trend is removed and all variability on the annual and subannual time scales is suppressed. Contour intervall 0.1 °C.

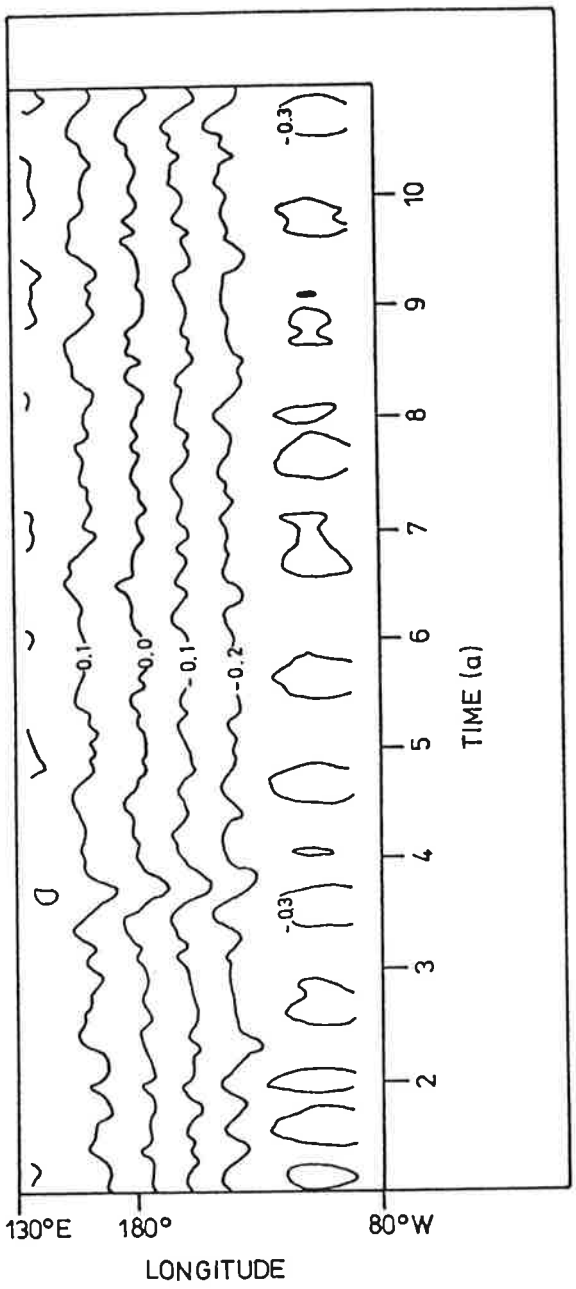

Figure 14:

Hovmøller diagram along the equator for simulated sea level. Contour interval 0.1 m.

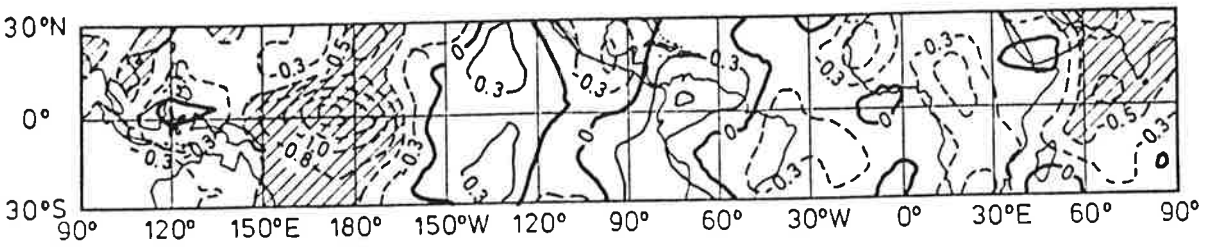

Figure 15:
Ratio, σ_c^2/σ_u^2, of 15-30 day DJF variance of 300 hPa velocity potential simulated by the coupled and by the uncoupled model. The reduction of the coupled run's variance, σ_c^2 compared to the variance σ_u^2, simulated with the uncoupled model is locally significant at the 95% level in stippled regions.

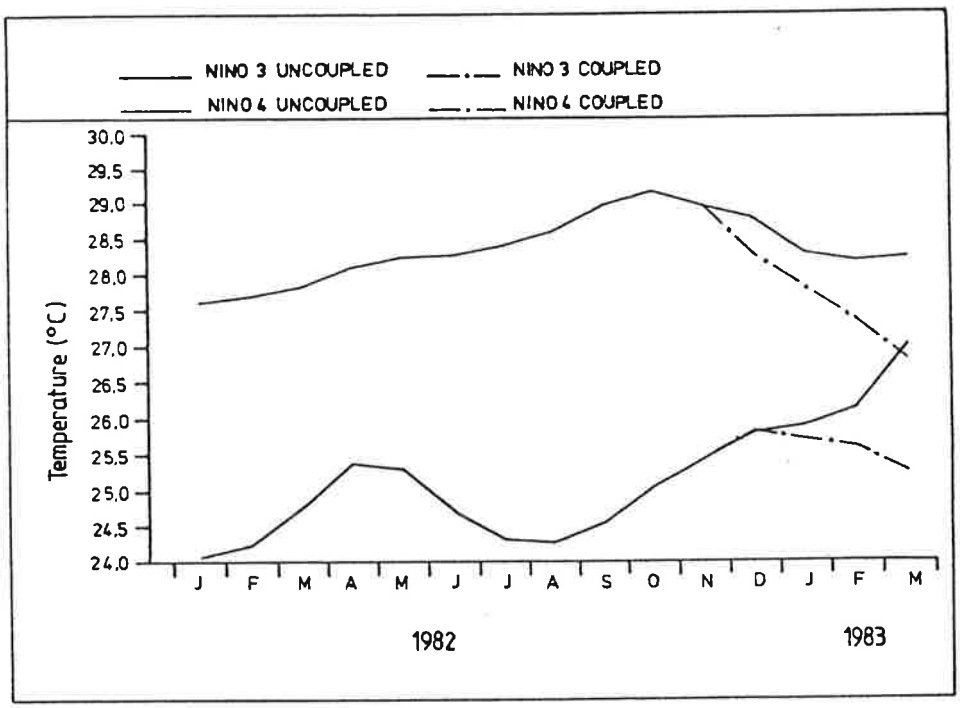

Figure 16:
Time evolution of SST in the Niño 3 (bottom) and Niño 4 (top) region, as calculated from the ocean model forced with observed winds (full lines) and as hindcasted by the coupled model using data up to December 1, 1982 (dashed dotted lines).

3.5 High Frequency Variability

Atmospheric variability in the "30-60" day frequency range is thought to be a possible trigger of ENSO events (Wyrtki, 1985). A "30-60" day type of wave is found in the upper air velocity potential simulated by the uncoupled atmospheric model. The model's wave propagates twice as fast as the observed wave does - its mean period is 21 days, but the spatial characteristics appear to be realistic (Storch et al., 1988). Therefore we compared 15-30 day variability of 300 hPa velocity potential simulated in the coupled and uncoupled simulations and subjected the differences to a local statistical test operating at a 5% significance level. The details of the test are given by Zwiers (1988).

The results for DJF, which are shown in Fig. 15, are typical of all seasons. The high frequency variation in the coupled simulation is significantly reduced in the convectively active region of the Equatorial Pacific between 150°E and the dateline. This is consistent with the picture of anomalous upper air confluence and reduced precipitation in this region due to the cooler equatorial Pacific which we have developed above. This reduction of high-frequency variability is perhaps one of the reasons why the simulated Equatorial Pacific displays such a small interannual variability.

4. SUMMARY AND DISCUSSION

We have conducted a ten year climate integration using a coupled oean-atmosphere general circulation model. The most important findings in this study are:

1) The simulated climate exhibits a significant climate trend, or drift. The trend is characterized by a cooling of the upper ocean in a latitude band which is centered on the equator and is a few degrees latitudes in width. The trend is almost linear after an initial more rapid drop in ocean temperature. The coupled atmosphere responds to these evolving boundary conditions in a manner which is reminiscent of an extended La Niña episode. Interestingly, the climate trend found in our coupled run is of opposite sign to that found by Gates et al. (1985) in their coupled simulation.

2) Inspite of the trend, the oceanic and atmospheric models, together with the flux correction strategy employed in the coupling algorithm, simulate the annual mean fields and the pattern and phase of the annual cycle with reasonable success. However, the amplitudes of seasonal changes are somewhat underestimated.

3) The coupled system's variability along the equator is reduced on all time scales. The energy of the atmospheric model's "30-60 day wave" is significantly reduced in the coupled system so that no westerly wind burst events take place in the Western Pacific. Possibly related to this lack of high-frequency variability is the absence of any noteworthy low-frequency variability of SST in our coupled integration. In particular, the model does not oscillate on the ENSO time scale of a few years.

The question arises, why does the model fail to simulate ENSO-like variability? There are several possible candidates to be blamed for the model's failure: a too strong damping of oceanic waves, the too diffusive modelled thermocline, the use of the flux-correction method, the cooling of the ocean and the severe underestimation of the atmospheric high-fequency variability.

In our ocean model waves are damped due to the choice of an implicit time step scheme. In such a scheme waves cannot propagate without being heavily

damped so that the "delayed negative feedback" mechanism (Graham and White, 1988) can not operate effectively. Wind burst experiments with the uncoupled ocean model show that SST anomalies in the Eastern equatorial Pacific caused by propagating Kelvin waves are of the order 0.2°C only, which are presumably too small to have a significant influence on the overlying atmosphere.

Another problem with the ocean model is its relatively diffusive thermocline, which results in weak sensitivity of Eastern Pacific SST to remote forcing. This model flaw further reduces the effect of Kelvin waves on SST in the Eastern Pacific.

A third critical point is the use of the flux correction technique when the dynamics of a system are not correctly simulated. The atmospheric model, when forced with observed SSTs, gives stress anomalies which are significantly weaker than the observed anomalies (Biercamp et al., 1988). For this reason ENSO prediction experiments with our coupled model failed completely. This is illustrated in Fig. 16, in which we display time series of simulated SST in the Niño 3 and Niño 4 regions in the Eastern and Western Pacific for two cases. In the first case the ocean model was run in an uncoupled mode and was forced with winds observed during the 1982/1983 ENSO event. The model clearly reproduced the warm event in this case. In the second case the coupled model was initialized with 1 December 1982 conditions using the method of Cane et al. (1986). At the time of initialization the warm event has already developed, at least in the Western Pacific (Niño 4 region). The coupled model, however, was unable to maintain the anomalous conditions and returned to normal very quickly. In order to keep the high SSTs, the atmospheric model had to generate intense westerly stress anomalies comparable to the observed anomalies. However, the simulated anomalies were only about half as large. As a consequence the total wind stress was still westward in the prediction experiment because of the applied momentum flux correction (Fig. 2b and c). Thus the equatorial upwelling continued and the SST anomalies were damped. These findings are similar to the results of Cane and Zebiak (1987), who showed that their prediction failed when the thermocline was raised by a certain amount and the equatorial heat content was consequently reduced significantly. Apparently the flux correction technique is not adequate for our purposes. A multiplicative correction technique may be better able to compensate for model defiencies than the additive method which we have used.

Air-sea interactions are not as energetic as they are in reality due to the cooling of the upper ocean layers . This may explain why the moderate SST anomaly which developed in the Western Pacific during year five (Fig. 13b) was not amplified by the atmospheric model. The anomalous heating of the atmosphere which resulted from this anomaly was simply too weak due to the already low temperatures. On the other hand, high frequency variability of the atmosphere over the Western Pacific is also reduced compared to the uncoupled case. This may also be attributed to the general cooling, which causes a weakening of convective activity in the Western Pacific (Fig. 6b and d) and a reduction of the energy of the "30-60 day" waves.

These arguments indicate that it is necessary to improve both the oceanic and atmospheric component of the coupled model. However, because there is still a long way to go in obtaining model fidelity, and because computing limitations will restrict us to relatively low horizontal and vertical resolution in both components of the model for some time to come, it is necessary to develop adequate coupling techniques which are able to overcome some of these problems.

Acknowledgements

The authors appreciate very much the assistance of U. Schlese and the staff of the Meteorologisches Institut at the Universität Hamburg in advising us on the use of the atmosphere model. The help of Prof. Dr. P. Speth from the Universität Köln is greatly acknowledged. Many thanks to Mrs. M. Grunert and Mr. M. Lüdecke for preparing the figures. The calculations were done on the Cyber 205 of the Deutsches Klimarechenzentrum in Hamburg.

5. REFERENCES

Barnston, A. G., and R. E. Livezey, 1987: Classification, seasonality and persistence of low-frequency atmospheric circulation patterns. **Mon. Wea. Rev.**, 115, 1083-126.

Biercamp, J. and H. v. Storch, 1987: Exchange of energy and momentum at the oceans surface. Climate simulations with the ECMWF t21 model in Hamburg, large scale atmospheric modelling, Report No. 1, G. Fischer Ed., Meteorologisches Institut der Universitaet, Bundesstr. 55, D 2000 Hamburg 13, F. R. G..

Biercamp, J., H. v. Storch, M. Latif, M. J Mc Phaden, and E. Kirk, 1988: Analyses of tropical anomalies simulated by a GCM. To be subm. to J. Atmos. Sci.

Cane, M.A., 1983: Oceanographic events during El Niño. **Science, 222,** 1189-1195.

Cane, M.A., S.E. Zebiak and S.C. Dolan, 1986: Experimental forecasts of El Niño. **Nature, 231,** 810-811.

Cane, M.A. and S.E. Zebiak, 1987: Prediction of El Niño events using a physical model. **Atmospheric and Oceanic Variability,** The Royal Meteorologial Society, Bracknell, U. K.

Cubasch, U., 1985: The mean response of the ECMWF global model to the El Nino anomaly in extended range prediction experiments. **Atmosphere-Ocean,** 23, 43-66.

Firring, E., R. Lucas, J. Sadler, and K. Wyrtki, 1983: Equatorial undercurrent disppears during 1982-1983 El Niño. **Science, 222,** 1121-1123.

Fischer, G., (Ed.) 1987: **Climate simulations with the ECMWF T21 model in Hamburg, Large scale atmospheric modelling, Report No. 1,** G. Fischer Ed., Meteorologisches Institut der Universitaet, Bundesstraße 55, D 2000 Hamburg 13, F.R.G.

Gates, W.L., Y.J. Han and M.E. Schlesinger, 1985: The global climate simulated by a coupled atmosphere-ocean general circulation model: preliminary results. **Coupled Ocean-Atmosphere Models,** J.C.J. Nihoul, Ed., Elsevier Oceanogr. Ser. 40.

Gill, A.E., 1980: Some simple solutions for heat-induced tropical circulation. **Quart. J. R. Met. Soc., 106,** 447-462.

Gill, A.E. and E.M. Rasmusson, 1983: The 1982-83 climate anomaly in the equatorial Pacific. **Nature, 306,** 229-234.

Goldenberg, S.O. and J.J. O'Brien, 1981: Time and space variability of tropical Pacific wind stress. **Mon. Wea. Rev., 109,** 1190-1207.

Graham, N.E. and W.B. White, 1988: The El Niño/Southern Oscillation as a natural oscillator of the tropical Pacific ocean/atmosphere system: Evidence from observations and models. Science, 240, 1293-1302.

Horel, J.D., 1982: On the annual cycle of the tropical Pacific atmosphere and ocean. **Mon. Wea. Rev., 110,** 1863-1878.

Latif, M., 1987: Tropical ocean circulation experiments. **J. Phys. Oceanogr., 17**, 246-263.

Latif, M., J. Biercamp, and H. von Storch, 1988: The response of a coupled ocean-atmosphere general circulation model to wind bursts. **J. Atmos. Sci., 45**, 964-979.

Pacanowski R.C. and S.G.H. Philander, 1981: Parameterization of vertical mixing in numerical models of tropical oceans. **J. Phys. Oceanogr., 11**, 1443-1451.

Sausen, R., K. Barthel and K. Hasselmann, 1987: Coupled ocean-atmosphere models with flux correction. **Climate Dynamics, 2**, 145-163.

Shea, D., 1986: Climatological Atlas: 1950-1979. Atmospheric Analysis and Prediction Devision. National Center for Atmospheric Research, Boulder Colorado, U. S. A..

Storch, H.v. (Ed.), 1988: **Climate Simulations with the ECMWF T21-model in Hamburg. Part II: Climatology and sensitivity experiments. Large Scale Atmospheric Modelling Report 4**, Meteorologisches Institut der Universität Hamburg, Bundesstraße 55, 2000 Hamburg 13, F.R.G..

Storch, H. v., T. Bruns, I. Fischer-Bruns, and K. Hasselmann, 1988: Principal Oscillation Pattern Analysis of the 30-60 day oscillation in a gcm equatorial troposhere. J. Geophys. Res., in press.

Weare, B.C., A.E. Navato, and R.E. Newell, 1976: Emperical orthoganal analysis of Pacific sea surface temperature. **J. Phys. Oceaongr., 6**, 671-678.

Wyrtki, K., 1974: The dynamic topography of the Pacific Ocean and its fluctuations. **HIG-74-5**, University of Hawaii, Honululu, U. S. A.

Wyrtki, K., 1985: Water displacements in the Pacific and the genesis of El Niño cycles. **J. Geophys. Res.,90**, 7129-7132.

Zebiak, S.E. and M.A. Cane, 1987: A model El Niño-Southern Oscillation. **Mon. Wea. Rev., 115**, 2262-2278.

Zwiers, F.W, 1988: **Aspects of the Statistical Analysis of Climate Experiments with Multiple Integrations**. Max Planck Institut für Meteorologie, Report No. 18. Max Planck Institut für Meteorologie, Bundesstraße 55, D 2000 Hamburg 13, F.R. Germany, 33pp.